

Control of threshold voltage in E-mode and D-mode GaN-on-Si metal-insulator-semiconductor heterostructure field effect transistors by in-situ fluorine doping of atomic layer deposition Al₂O₃ gate dielectrics

J. W. Roberts, P. R. Chalker, K. B. Lee, P. A. Houston, S. J. Cho, I. G. Thayne, I. Guiney, D. Wallis, and C. J. Humphreys

Citation: *Appl. Phys. Lett.* **108**, 072901 (2016); doi: 10.1063/1.4942093

View online: <http://dx.doi.org/10.1063/1.4942093>

View Table of Contents: <http://aip.scitation.org/toc/apl/108/7>

Published by the [American Institute of Physics](#)

Articles you may be interested in

[On the physical operation and optimization of the p-GaN gate in normally-off GaN HEMT devices](#)
Applied Physics Letters **110**, 123502 (2017); 10.1063/1.4978690

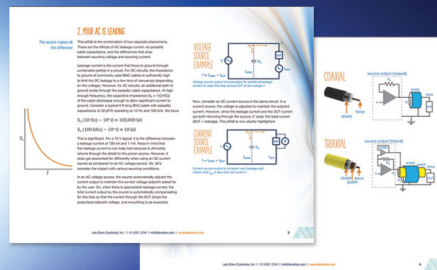
[Threshold voltage control by gate oxide thickness in fluorinated GaN metal-oxide-semiconductor high-electron-mobility transistors](#)
Applied Physics Letters **103**, 033524 (2013); 10.1063/1.4815923

[The physical mechanism on the threshold voltage temperature stability improvement for GaN HEMTs with pre-fluorination argon treatment](#)
Applied Physics Letters **108**, 233507 (2016); 10.1063/1.4953573

[Investigation of gate leakage current mechanism in AlGaIn/GaN high-electron-mobility transistors with sputtered TiN](#)
Journal of Applied Physics **121**, 044504 (2017); 10.1063/1.4974959

[Normally-off p-GaN/AlGaIn/GaN high electron mobility transistors using hydrogen plasma treatment](#)
Applied Physics Letters **109**, 152106 (2016); 10.1063/1.4964518

[Interface/border trap characterization of Al₂O₃/AlN/GaN metal-oxide-semiconductor structures with an AlN interfacial layer](#)
Applied Physics Letters **106**, 051605 (2015); 10.1063/1.4907861



5 Electronic Measurement Pitfalls to Avoid

Get the whitepaper

Control of threshold voltage in E-mode and D-mode GaN-on-Si metal-insulator-semiconductor heterostructure field effect transistors by *in-situ* fluorine doping of atomic layer deposition Al₂O₃ gate dielectrics

J. W. Roberts,¹ P. R. Chalker,¹ K. B. Lee,² P. A. Houston,² S. J. Cho,³ I. G. Thayne,³ I. Guiney,⁴ D. Wallis,⁴ and C. J. Humphreys⁴

¹Centre for Materials and Structures, University of Liverpool, Liverpool L69 3GH, United Kingdom

²Electronic and Electrical Engineering, University of Sheffield, Sheffield S1 3JD, United Kingdom

³School of Engineering, University of Glasgow, Glasgow G12 8LT, United Kingdom

⁴Materials Science and Metallurgy, University of Cambridge, Cambridge CB3 0FS, United Kingdom

(Received 23 September 2015; accepted 4 February 2016; published online 16 February 2016)

We report the modification and control of threshold voltage in enhancement and depletion mode AlGaIn/GaN metal-insulator-semiconductor heterostructure field effect transistors through the use of *in-situ* fluorine doping of atomic layer deposition Al₂O₃. Uniform distribution of F ions throughout the oxide thickness are achievable, with a doping level of up to $5.5 \times 10^{19} \text{ cm}^{-3}$ as quantified by secondary ion mass spectrometry. This fluorine doping level reduces capacitive hysteretic effects when exploited in GaN metal-oxide-semiconductor capacitors. The fluorine doping and forming gas anneal also induces an average positive threshold voltage shift of between 0.75 and 1.36 V in both enhancement mode and depletion mode GaN-based transistors compared with the undoped gate oxide via a reduction of positive fixed charge in the gate oxide from $+4.67 \times 10^{12} \text{ cm}^{-2}$ to $-6.60 \times 10^{12} \text{ cm}^{-2}$. The application of this process in GaN based power transistors advances the realisation of normally off, high power, high speed devices. © 2016 AIP Publishing LLC. [<http://dx.doi.org/10.1063/1.4942093>]

The development of AlGaIn/GaN based power transistors is the focus of widespread research as they offer the potential for large efficiency savings when used in power switching applications compared to Si and SiC based devices.^{1,2} The basis of these devices is the utilisation of a high mobility 2-dimensional electron gas (2DEG) underneath the AlGaIn/GaN interface which allows rapid switching and low on-resistance transistors to be fabricated for power control applications.

For power transistor applications, it is desirable to have normally off devices.³ One way to achieve this is to form a negative charge in the gate region of the device by doping or ion implantation with fluorine (F) ions in the gate region of the device.³⁻⁷ Alternative fluorine treatments have been investigated elsewhere, as a means of ameliorating the relatively high defect densities associated with atomic layer deposition (ALD) of amorphous Al₂O₃-nitride device structures.⁸ A fluorine-based plasma treatment has been previously described as a method of incorporating negatively charged F ions into the AlGaIn barrier of an E-mode high electron mobility transistor (HEMT) and resulted in a positively shifted threshold voltage.⁹

Further development of normally off AlGaIn/GaN MISHEMT devices was achieved by exploiting fluorinated Al₂O₃ thin film gate dielectrics, prepared using the fluorine-based plasma treatment. The E-mode MISHEMTs exhibited high transconductance (153 mS/mm) and large saturated drain currents (547 mA/mm) when the plasma treatment was performed on the dielectric surface.¹⁰ It was reported that the F-distribution was confined to the top 2 nm of the dielectric and furthermore avoided plasma-induced damage at the interface with the III-nitride. Zhang *et al.*⁴ have reported the compensation of the intrinsic positive charges in Al₂O₃ gate

dielectric by fluorine ions incorporated into the Al_{0.26}Ga_{0.74}N barrier of GaN metal-oxide-semiconductor high-electron-mobility transistors (MOSHEMTs) by CF₄ plasma treatment. The incorporated fluorine redistributed by diffusion back into the Al₂O₃ during ALD at 250 °C, although a further post-deposition anneal at 400 °C left the F-distribution almost unchanged. Here, we report an *in-situ* process for the uniform F doping of alumina throughout the gate oxide thickness deposited by atomic layer deposition. This approach avoids exposure of the III-nitride to detrimental effects from plasma treatment and reduces the overall thermal budget during fabrication.

Substrates for the electrical properties characterisation were grown by MOCVD on 6" Si(111) wafers. For metal-oxide-semiconductor capacitor (MOSC) substrates, the layer structure consisted of Si(111)/AlN nucleation layer/graded AlGaIn layer/n-GaN doped with $1 \times 10^{18} \text{ cm}^{-3}$ Si/n-GaN doped with $1 \times 10^{17} \text{ cm}^{-3}$ Si. Planar circular MOSC structures were fabricated utilising Ti/Al/Ni/Au ohmic contacts in contact with the $1 \times 10^{18} \text{ cm}^{-3}$ Si doped layer and annealed at 770 °C for 30 s in N₂. Following a cleaning step using acetone and IPA, ~10 nm Al₂O₃ and a range of concentrations of F:Al₂O₃ were deposited onto different MOSC substrates using the ALD processes described further on in this paper. After ALD, windows through the dielectric layer were opened over the ohmic contacts using a SiCl₄ reactive-ion etch. Ni/Au pads were deposited to form the top contacts of the MOSC structures. Completed MOSC structures were annealed at 430 °C in forming gas (90%N₂/10%H₂) for 30 min to improve the interface quality.¹¹

Substrates for the MISHFET devices consisted of Si(111)/AlN nucleation layer/graded AlGaIn layer/C doped GaN at $5 \times 10^{18} \text{ cm}^{-3}$ /undoped GaN/1 nm AlN/27 nm

AlGaN/2 nm GaN. Hall measurements of the substrates yielded sheet resistance of $490 \Omega/\square$, sheet carrier density of $6.9 \times 10^{12} \text{ cm}^{-2}$, and electron mobility of $1855 \text{ cm}^2/\text{V s}$. The devices were processed by mesa etching, ohmic formation, SiN_x passivation, gate foot opening, F ion implantation¹² (for E-mode only), Al_2O_3 or F: Al_2O_3 gate deposition, 30 min forming gas anneal (FGA) at 430°C , T-gate formation, and probe pad formation. The gate lengths and gate widths for the MISHFET devices were $1.5 \mu\text{m}$ and $100 \mu\text{m}$, respectively, and each coupon was approximately $10 \times 10 \text{ mm}$.

Atomic layer deposition was used to grow the F: Al_2O_3 and Al_2O_3 films presented in this paper. The growth of all ALD films was carried out using an Oxford Instruments Plasma OpAL reactor. Substrate temperatures were set at 200°C for the depositions. The initial depositions were made onto Si(100) substrates for characterisation by spectroscopic ellipsometry (SE) and secondary ion mass spectroscopy (SIMS). For undoped control samples, cycles of trimethyl aluminium (TMA) and H_2O were used in the standard Al_2O_3 thermal process. Each cycle for this process consisted of 0.02 s TMA - 3 s 100 sccm Ar purge - 0.01 s H_2O - 3 s 100 sccm Ar purge. F: Al_2O_3 was deposited using a similar recipe in which the H_2O precursor was replaced with a 40% $\text{NH}_4\text{F}:\text{H}_2\text{O}$ solution. Each cycle consisted of: 0.02 s TMA - 3 s 100 sccm Ar purge - 0.01 s $\text{NH}_4\text{F}:\text{H}_2\text{O}$ - 3 s 100 sccm Ar purge. 500 growth cycles were used for SE characterisation while substrates prepared for SIMS used 1000 cycles. For fixed charge analysis, the ALD oxide samples were grown on MOSC substrates with a range of F concentrations. This was achieved by replacing H_2O pulses with 40% $\text{NH}_4\text{F}:\text{H}_2\text{O}$ pulses evenly throughout the oxide growth. For example, the 10% F cycle recipe comprised of 9 standard TMA/ H_2O cycles followed by 1 TMA/ $\text{NH}_4\text{F}:\text{H}_2\text{O}$ cycle, repeated until the required thickness was achieved. Throughout the rest of this paper F: Al_2O_3 refers to oxides grown with 100% of the H_2O pulses replaced with $\text{NH}_4\text{F}:\text{H}_2\text{O}$ pulses.

SE was used for characterisation of the films grown on Si(100) before and after (FGA) at 430°C in 10% H_2 /90% N_2 with a scan range of 500–750 nm. Fitting was performed using a new amorphous model for Al_2O_3 to determine the film thicknesses and the refractive index of the material. Equation (1) shows the single term Sellmeier dispersion formula¹³

$$n^2(\lambda) - 1 = S_0 \lambda_0^2 / [1 - (\lambda_0/\lambda)^2]. \quad (1)$$

The average oscillator strength, S_0 and the average oscillator position, λ_0 can be obtained by plotting $1/(n^2 - 1)$ versus $1/\lambda^2$. The slope of the resultant straight line gives $1/S_0$ while the intercept at infinite wavelength yields $1/S_0 \lambda_0^2$. An alternative form of the equation allows the average single oscillator energy gap to be calculated¹⁴

$$n^2 - 1 = E_d E_0 / (E_0^2 - (\hbar\omega)^2), \quad (2)$$

where $\hbar\omega$ = photon energy, E_0 = the average single oscillator energy gap in eV, and E_d = the average oscillator strength in eV.

Further characterisation was conducted on 1000 cycle films deposited on Si(100) using SIMS. SRIM modelling and

a 35 keV F ion implanted $\sim 100 \text{ nm}$ Al_2O_3 on Si(100) were used to enable quantification of the *in-situ* doped oxide.

Figure 1 shows the SE results for the calculation of the single oscillator Sellmeier average oscillator strength, average oscillator position, and average oscillator energy gap. Refractive indices at 632.8 nm were found to be 1.655 for as grown Al_2O_3 and 1.657 after FGA, within the expected range for thin film Al_2O_3 grown by other groups.^{15,16} Replacing the H_2O dose with 40% $\text{NH}_4\text{F}:\text{H}_2\text{O}$ reduced the refractive index at 632.8 nm to 1.646. This value was further reduced to 1.644 with the application of FGA. The slight increase in n after FGA for the undoped film could be attributed to either the film becoming denser as a result of the heat treatment,¹⁵ the forming gas passivating unsatisfied positive bonds in the oxide¹⁷ or a combination of the two. The reduction in n seen with the addition of 40% $\text{NH}_4\text{F}:\text{H}_2\text{O}$ indicated that Al-F bonds could be present in the material. Since AlF_3 has a significantly lower n than Al_2O_3 at 1.2–1.4 (Refs. 18 and 19), a lower refractive index would be expected if a mixed amorphous material consisting of Al-O and Al-F bonds was being produced. However, as the reduction in n was only of the order of 10^{-2} , this indicated that the F content of the films was low. Following the FGA, the slight reduction seen in the refractive index for F: Al_2O_3 could be attributed to displacement of O for F within the oxide^{4,20} or by a change in density of the films. Figure 1 shows the results for the average oscillator strength, S_0 , the average oscillator position, λ_0 , the average single oscillator energy gap in eV, E_0 , and the average oscillator strength in eV, E_d . The average oscillator strength was found to reduce by the addition of F into the oxide from $1.919 \times 10^{14} \text{ m}^{-2}$ to $1.862 \times 10^{14} \text{ m}^{-2}$. This was attributed to the replacement of a proportion of the Al-O dipoles with higher mass Al-F dipoles.²¹ The average oscillator positions were found to be 94.1 nm for Al_2O_3 and 94.7 for F: Al_2O_3 . The resonant frequency ω_0 is inversely related to the average oscillator position by

$$\omega_0 = 2\pi c / \lambda_0, \quad (3)$$

where c = velocity of light in free space. Furthermore

$$\omega_0 = \sqrt{k/M}, \quad 1/M = (1/M_-) + (1/M_+), \quad (4)$$

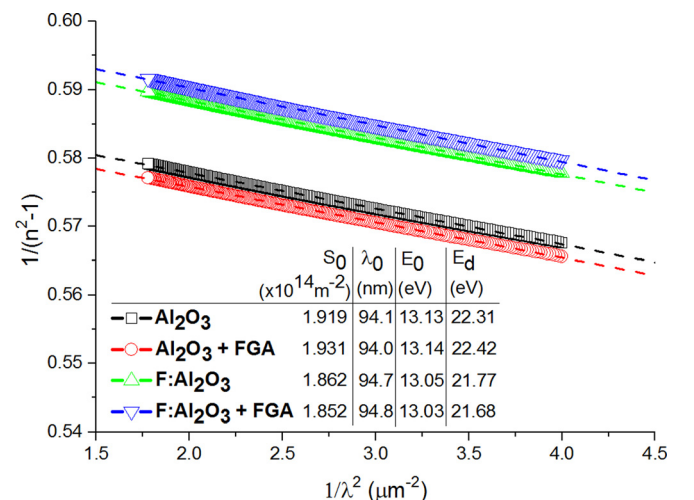


FIG. 1. Sellmeier average single oscillator strengths for Al_2O_3 and F: Al_2O_3 before and after forming gas anneal.

where k = the spring constant, M , M_- , and M_+ are the reduced mass and negative and positive ion masses, respectively.¹⁹ In their analysis, M_+ represents the Al atomic mass, and M_- represents either the negatively charged F or O atomic masses. The increase in λ_0 (and decrease in ω_0) implies that the reduced mass term, M , is increased by the addition of F into the oxide. As the positive Al mass should be unchanged, this increase in M can be attributed to the change from lighter O atoms to heavier F atoms. As ALD Al_2O_3 grown by thermal methods is known to possess intrinsic positive bulk charge,⁴ this Sellmeier analysis indicates that the increase in F, with its additional electron and higher electronegativity compared to O,⁷ and the effect of the FGA could compensate for the native positive charge that occurs in ALD Al_2O_3 .

Figure 2 shows the results of SIMS analysis for ~ 100 nm of Al_2O_3 F ion implanted with a 35 keV ion beam and from the *in-situ* doped oxide. SIMS results for the *in-situ* doped oxide show a F concentration of $\sim 5.5 \times 10^{19} \text{ cm}^{-3}$, which based on Al_2O_3 density between 3 g/cm^3 (Ref. 15) and 3.95 g/cm^3 yields a F concentration of between 0.06 at. % and 0.05 at. %, in agreement with that detected using XPS (not shown). The doping profile as observed using SIMS showed a uniform doping density throughout the oxide with slight increases in doping concentration at the upper and lower interfaces.

Figure 3(a) shows the MOSC results of 1 MHz capacitance-voltage sweeps at room temperature for ~ 10 nm of Al_2O_3 and the same thickness of F: Al_2O_3 . In the undoped sample, the flat band voltage (V_{FB}) was ~ 0.5 V, and hysteresis was ~ 1 V. V_{FB} and C_{FB} were determined from the inflection points of the CV plot in accordance with Ref. 22. In the 100% F doped sample, V_{FB} shifted positively to ~ 2.5 V (a shift of +2 V) while the hysteresis was reduced to ~ 0.5 V. Chakroun *et al.*²³ summarise recent work on hysteresis reduction via use of surface cleaning processes and alternative surface passivation techniques on GaN. They show that

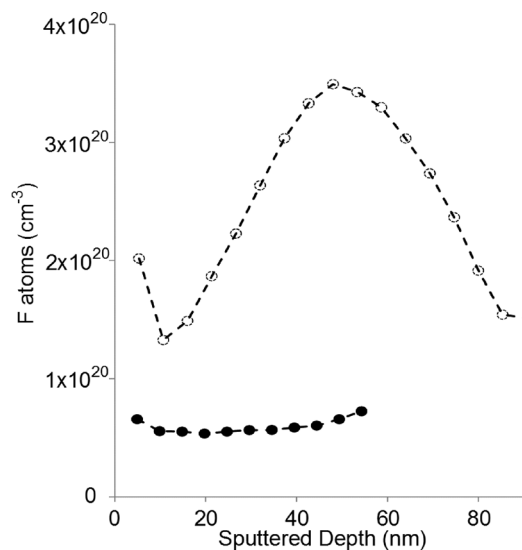


FIG. 2. SIMS depth profile of a 35 keV F ion implanted ALD Al_2O_3 film (open circles) and corresponding SIMS profile for *in-situ* doped F: Al_2O_3 (closed circles).

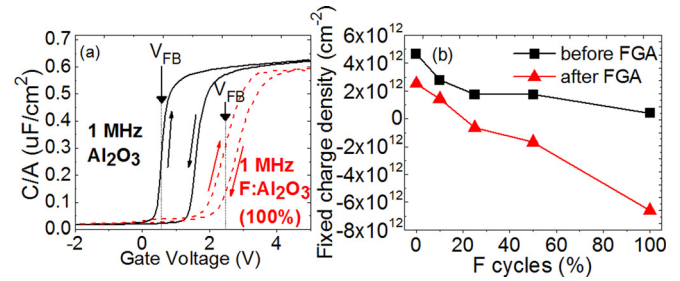


FIG. 3. (a) 1 MHz CV showing hysteresis and flat band voltage for Al_2O_3 and F: Al_2O_3 . (b) Fixed charge against percentage of fluorine cycles before and after forming gas anneal.

depending on the type of passivation layer used, hysteresis can range from <0.1 V (Ref. 24) to 10 V.²⁵ The best value they reported after optimisation of the surface treatment prior to gate deposition was 0.2 V. The reduction in hysteresis seen here was thought to come from negatively charged F atoms within the bulk oxide compensating for residual intrinsic positive traps resulting from the growth process, as shown in Figure 3(b). Figure 3(b) shows the fixed charge within the gate dielectric as calculated from the CV results.²⁶ Without FGA, the number of fixed charges in the undoped Al_2O_3 is $+4.67 \times 10^{12} \text{ cm}^{-2}$. With the addition of NH_4F into the ALD growth process, the positive fixed charges are compensated for. Increasing the percentage of F in the oxide serves to further reduce the positive fixed charge up to a maximum reduction of around one order of magnitude ($+4.67 \times 10^{12} \text{ cm}^{-2}$ to $+4.04 \times 10^{11} \text{ cm}^{-2}$). After FGA, the bulk charge for Al_2O_3 is halved to $+2.53 \times 10^{12} \text{ cm}^{-2}$. The influence of the F doping process is increased following FGA, with the 100% F: Al_2O_3 showing negative bulk charge at $-6.60 \times 10^{12} \text{ cm}^{-2}$.

The positive shift in V_{FB} can be attributed to the higher concentration of negative charges near to the n-GaN/dielectric interface, introduced by the F doping as evidenced in Figure 3(b) and implicated by the Sellmeier analysis above. Undoped Al_2O_3 and 100% F: Al_2O_3 were subsequently incorporated within E- and D-mode MISHFET fabrication processes to ascertain the effect of the gate oxide in GaN-on-Si MISHFET devices.

Figure 4(a) shows drain current (I_{D}) against gate source voltage (V_{GS}) and the gate leakage current (I_{G}) for representative D-mode MISHFET devices with 20 nm Al_2O_3 and 20 nm F: Al_2O_3 gate oxides and gate to drain distances of 12 μm . 15 devices of each type were measured for the data reported here. All devices tested were found to work, and no relationship between device location and HEMT properties is observed. The maximum drain current is unaffected by the addition of F into the gate oxide layer with both sets of devices giving I_{Dmax} between 600 and 800 mA/mm. The threshold voltage (V_{TH}) for the standard undoped gate oxide devices ranges from -9.39 V to -8.86 V, with a mean V_{TH} of -9.23 V. With the addition of F into the gate stack measurements across several devices give mean V_{TH} values of -8.48 V, an increase in $+0.75$ V, with values ranging from -8.65 V to -8.10 V. Gate leakage currents are of the order of 1×10^{-6} mA/mm for both oxides, although a small proportion of the devices showed higher gate leakage up to

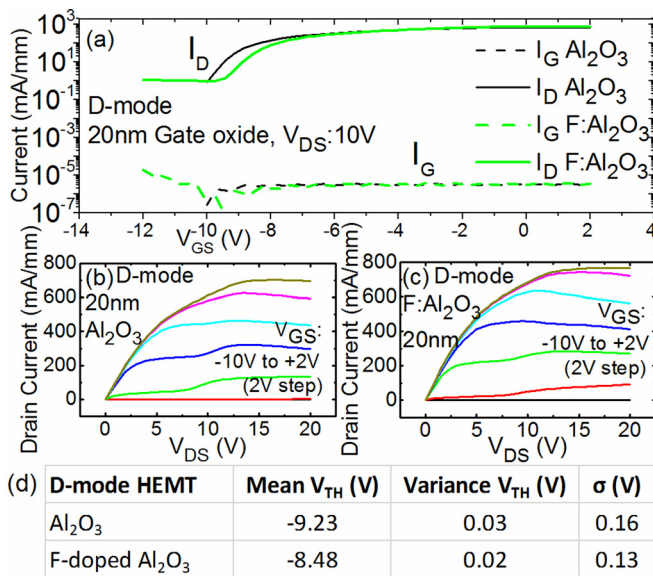


FIG. 4. D-mode devices (a) I_D and I_G against V_{GS} for 20 nm Al_2O_3 and F: Al_2O_3 . (b) I_D against V_{DS} for 20 nm Al_2O_3 gate oxide with V_{GS} from $-10V$ to $+2V$ in 2V steps. (c) I_D against V_{DS} for 20 nm F: Al_2O_3 gate oxide with V_{GS} from $-10V$ to $+2V$ in 2V steps. (d) Mean, variance, and standard deviation (σ) of V_{TH} for 15 of each type of MISHFET.

1×10^{-3} mA/mm. Devices with the higher gate leakage still showed consistent V_{TH} and I_{Dmax} values. Figures 4(b) and 4(c) show the drain current characteristics for both sets of devices and shows kinks in the drain current between 8 and $10V_{DS}$. This is thought to be related to the presence of slow traps in the GaN buffer layer within the substrate.²⁷ The peak transconductance for both sets range from 120 to 128 mS/mm. The mean, variance, and standard deviation (σ) of V_{TH} for 15 of each type of MISHFET are shown in Figure 4(d). The mean shift in V_{TH} is observed to be 0.75 V due to the F-doping of the alumina gate dielectric in the D-mode devices. The F-induced shift is statistical significant with a 99% confidence limit as determined by a t-test.

Figure 5(a) shows I_D and I_G against V_{GS} for a representative E-mode MISHFET (produced by the ion implantation of F into the barrier as described elsewhere in Ref. 12) with both 20 nm Al_2O_3 and 20 nm F: Al_2O_3 gate oxides. I_{Dmax} for the standard Al_2O_3 gate dielectric range from 400 to 500 mA/mm across all devices tested. This is slightly reduced in the F: Al_2O_3 devices to around 350–400 mA/mm. Mean V_{TH} for the Al_2O_3 gated device is $+0.99$ V. The maximum and minimum V_{TH} values are $+1.83$ V and $+0.10$ V, respectively. With the addition of the *in-situ* deposited F, the mean V_{TH} value is found to increase to $+2.35$ V, an increase in $+1.36$ V, with values ranging from $+1.97$ V to $+2.60$ V. The addition of F into the gate oxide layer also reduces the off-state drain current for gate-source voltages below V_{TH} compared to the standard Al_2O_3 gate oxide. Figures 5(b) and 5(c) show the drain current characteristics for E-mode devices with standard ALD Al_2O_3 and *in-situ* doped F: Al_2O_3 . Peak transconductance for E-mode devices with Al_2O_3 gate dielectric range from 65 to 95 mS/mm and 70 to 90 mS/mm for E-mode devices with F: Al_2O_3 gate dielectric. Figure 5(d) shows the mean, variance, and standard deviation (σ) of V_{TH} for 15 of each type of MISHFET. Fluorine-doping of alumina gate dielectric causes

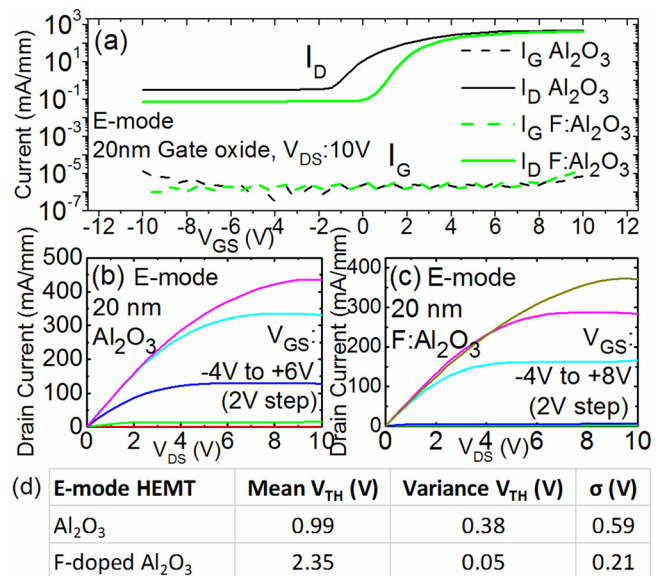


FIG. 5. E-mode devices (a) I_D and I_G against V_{GS} for 20 nm Al_2O_3 and F: Al_2O_3 . (b) I_D against V_{DS} for 20 nm Al_2O_3 gate oxide with V_{GS} from $-4V$ to $+6V$ in 2V steps. (c) I_D against V_{DS} for 20 nm F: Al_2O_3 gate oxide with V_{GS} from $-4V$ to $+8V$ in 2V steps. (d) Mean, variance, and standard deviation (σ) of V_{TH} for 15 of each type of MISHFET.

a shift in the mean V_{TH} of 1.36 V for the E-mode devices. The statistical significance of the F-induced shift has a 99% confidence limit as determined by a t-test. Although direct comparisons between results from different groups are awkward due to differences in device layout, processing steps, etc., recent advances and publications in the field for D- and E-mode GaN-based MISHFET devices show that higher drain currents and peak transconductances are achievable (1550 mA/mm and 330 mS/mm, respectively, for the D-mode,²⁸ and 1130 mA/mm (Ref. 29) and 153 mS/mm for E-mode¹⁰) through further device optimisation.

In conclusion, positive V_{FB} and V_{TH} shifts in GaN-on-Si MOSCs and GaN-on-Si MISHFETs were demonstrated via atomic layer deposition *in-situ* doping and growth of Al_2O_3 gate oxide with F. This was achieved using a 40% $NH_4F:H_2O$ precursor in place of the standard H_2O precursor. Spectroscopic ellipsometry results, single oscillator Sellmeier analysis, and fixed charge calculations from MOSC CV analysis showed that increasing levels of F compensated for positive traps in the oxide. Following gate deposition, annealing in 10% $H_2/90\%N_2$ increased the effect of the F, resulting in a maximum fixed negative charge of $-6.6 \times 10^{12} cm^{-2}$. SIMS results showed that the doping of F in Al_2O_3 gave a more uniform concentration of F atoms through the oxide compared to other methods such as ion implantation, with a doping concentration around $5.5 \times 10^{19} cm^{-3}$. In total, 60 MISHFET devices were measured. 30 E-mode and D-mode devices were produced, with half of each device type using Al_2O_3 gate oxide and the other half using F: Al_2O_3 gate oxide. The mean D- and E-mode V_{TH} shifts due to F-incorporation were found to be 0.75 V and 1.36 V, respectively, with a confidence limit of 99%. F: Al_2O_3 gate oxide can be used in conjunction with other E-mode MISHFET methods, such as ion implantation, gate recess, tri-gate to achieve devices with more positive V_{TH} , and low gate leakage currents.

This work has been supported by the Engineering and Physical Sciences Research Council Programme Grant No. EP/K014471/1 “Silicon Compatible GaN Power Electronics.” Data files for the figures in this paper may be accessed at <http://datacat.liverpool.ac.uk/id/eprint/60>.

- ¹S. Dimitrijević, J. Han, H. A. Moghadam, and A. Aminbeidokhti, *Mater. Res. Soc. Bull.* **40**, 399 (2015).
- ²G. Ghione, K. J. Chen, T. Egawa, G. Meneghesso, T. Palacios, and R. Quay, *IEEE Trans. Electron Devices* **60**, 2975 (2013).
- ³S. Chowdhury and U. K. Mishra, *IEEE Trans. Electron Devices* **60**, 3060 (2013).
- ⁴Y. Zhang, M. Sun, S. J. Joglekar, T. Fujishima, and T. Palacios, *Appl. Phys. Lett.* **103**, 033524 (2013).
- ⁵W. Chong, C. Chong, H. Yunlong, Z. Xuefeng, M. Xiaohua, Z. Jincheng, M. Wei, and H. Yue, *J. Semicond.* **35**, 014008 (2014).
- ⁶M. J. Wang, L. Yuan, K. J. Chen, F. J. Xu, and B. Shen, *J. Appl. Phys.* **105**, 083519 (2009).
- ⁷S. Huang, H. Chen, and K. J. Chen, *Appl. Phys. Lett.* **96**, 233510 (2010).
- ⁸S. Gu, E. A. Chagarov, J. Min, S. Madisetti, S. Novak, S. Oktyabrsky, A. J. Kerr, T. Kaufman-Osborn, A. C. Kummel, and P. M. Asbeck, *Appl. Surf. Sci.* **317**, 1022 (2014).
- ⁹Y. Cai, Y. Zhou, K. M. Lau, and K. J. Chen, *IEEE Trans. Electron Devices* **53**, 2207 (2006).
- ¹⁰C. Chen, X. Liu, B. Tian, P. Shu, Y. Chen, W. Zhang, H. Jiang, and Y. Li, *IEEE Electron Device Lett.* **32**, 1373 (2011).
- ¹¹Y.-C. Yoon, K.-S. Park, and S.-D. Kim, *Mater. Sci. Semicond. Process.* **34**, 343 (2015).
- ¹²K. B. Lee, I. Guiney, S. Jiang, Z. H. Zaidi, H. Qian, D. J. Wallis, M. J. Uren, M. Kuball, C. J. Humphreys, and P. A. Houston, *Appl. Phys. Express* **8**, 036502 (2015).
- ¹³M. DiDomenico, Jr. and S. H. Wemple, *J. Appl. Phys.* **40**, 720 (1969).
- ¹⁴R. D. Shannon, R. C. Shannon, O. Medenback, and R. X. Fischer, *J. Phys. Chem. Ref. Data* **31**, 931 (2002).
- ¹⁵M. D. Groner, F. H. Fabreguette, J. W. Elam, and S. M. George, *Chem. Mater.* **16**, 639 (2004).
- ¹⁶P. Kumar, M. K. Wiedmann, C. H. Winter, and I. Avrutsky, *Appl. Opt.* **48**, 5407 (2009).
- ¹⁷V. Djara, K. Cherkaoui, M. Schmidt, S. Monaghan, É. O’Connor, I. M. Povey, D. O’Connell, M. E. Pemble, and P. K. Hurley, *IEEE Trans. Electron Devices* **59**, 1084 (2012).
- ¹⁸S. Pat, N. E. Çetin, N. Ekem, M. Z. Balbag, and Ş. Korkmaz, *Mater. Focus* **3**, 72 (2014).
- ¹⁹B.-H. Liao, C.-C. Lee, C.-C. Jaing, and M.-C. Liu, *Opt. Rev.* **16**, 505 (2009).
- ²⁰S. E. Kim and Ch. Steinbrüchel, *Appl. Phys. Lett.* **75**, 1902 (1999).
- ²¹C. S. Lai, K. M. Fan, H. K. Peng, S. J. Lin, C. Y. Lee, and C. F. Ai, *Appl. Phys. Lett.* **90**, 172904 (2007).
- ²²R. Winter, J. Ahn, P. C. McIntyre, and M. Eizenberg, *J. Vac. Sci. Technol. B* **31**, 030604 (2013).
- ²³A. Chakroun, H. Maher, E. A. Alam, A. Souifi, V. Aimez, R. Ares, and A. Jaouad, *IEEE Electron Device Lett.* **35**(3), 318 (2014).
- ²⁴C. Bae and G. Lucovsky, *J. Vac. Sci. Technol. A* **22**(6), 2379 (2004).
- ²⁵P. Chen, W. Wang, and S. J. Chua, *Appl. Phys. Lett.* **79**(21), 3530 (2001).
- ²⁶D. K. Schroder, *Semiconductor Material and Device Characterization* (IEEE Press, Wiley-Interscience, 2006), ISBN: 978-0-471-73906-7.
- ²⁷G. Meneghesso, F. Zanoni, M. J. Uren, and E. Zanoni, *IEEE Electron Device Lett.* **30**, 100 (2009).
- ²⁸J. Ma, X. Lu, X. Zhu, T. Huang, J. Huaxing, P. Xu, and K. M. Lau, *J. Cryst. Growth* **414**, 237 (2014).
- ²⁹S. Huang, X. Liu, J. Zhang, K. Wei, G. Liu, X. Wang, Y. Zheng, H. Liu, Z. Jin, C. Zhao, C. Liu, S. Liu, S. Yang, J. Zhang, Y. Hao, and K. J. Chen, *IEEE Electron Device Lett.* **36**(8), 754 (2015).